2024 IEEE/RSJ International Conference on Intelligent Robots and Systems (IROS)
October 14-18, 2024. Abu Dhabi, UAE

Data-Driven Modeling of Cable Slab Dynamics via Neural Networks

Yazan M. Al-Rawashdeh[1] Mohammad Al Saaideh[2] Michael Pumphrey[3]
Natheer Alatawneh[2] Mohammad Al Janaideh[2,3,4]

***Abstract*— A novel method for analyzing the dynamics and bend geometry of a cable slab via trained neural networks is introduced. Neural networks are trained from real-time visual feedback capture via a high-speed camera during cyclic motion to track the positions of multiple markers affixed to the cable slab through image processing techniques. Experimental parameters are systematically varied to ensure a diverse range of training patterns. Consequently, two distinct data-driven neural network models are developed: a coupled model and a decoupled model. These models accurately predict the two-dimensional positions of the markers, even during non-cyclic motion profiles. Subsequently, the marker positions are utilized as waypoints to generate a cubic spline curve with time-varying coefficients, approximating the spatiotemporal solution of the cable slab dynamics. Notably, this spline can be segmented into smaller sections tailored to specific research objectives. Experimental results validate the effectiveness of the proposed methodology.**

I. Introduction

Multi-directional movement occurs through both linear and angular motions in many motion system applications. For instance, wafer scanners utilized in semiconductor manufacturing achieve such multi-directional motion through the coordination and synchronization of positioning stages [1]–[3]. Typically, these stages are mechanically linked, necessitating flexible cable slabs to house cable harnesses for signal and power transmission, as well as hose assemblies for fluid conveyance. This mechanical interconnection establishes dynamic links, resulting in residual vibration, reaction forces, and coupling between the positioning stages, potentially leading to degradation in tracking performance [4]. Accurate models or estimates of these forces are crucial for improving positioning performance, mitigating springback, and understanding hose and cable bending behaviors [5], [6]. However, the large nonlinear deformations experienced by cable slabs during motion pose challenges for mathematical modeling [6]. Consequently, obtaining information about reaction forces is often impractical. Nonetheless, various mathematical modeling techniques for flexible pipes and hoses have been documented in the literature, including finite element analysis as a common approach [6]–[8]. Alternatively, data-driven techniques can be employed to estimate cable slab-induced reaction forces, which can then be utilized in feedforward compensation control schemes, such as lookup tables-based approaches [9].

Repetive movement of the cable slab's motion profiles, both cyclic and acyclic, impact its bending geometry. This, in turn, leads to loading cycles responsible for creating fatigue-induced micro-cracks [6], [9], [10]. As a consequence, hose leakage may occur, and the cable harnesses could suffer damage [10]–[12]. Therefore, predicting the lifespan of cable slab assemblies becomes crucial for planning scheduled maintenance to minimize system downtime. Furthermore, during motion, the bend geometry of the cable slab may form a hump, necessitating careful consideration when allocating clearance between interacting positioning stages. Compliance with the manufacturer's specified minimum bend radius is essential. Moreover, the varying bend geometry resulting from cable slab motion may introduce vertical disturbance forces and pressure level variations in air bearing, contributing to vertical positioning errors [13]. Mathematical models of cable slab dynamics, whether in nodal or absolute coordinates, often manifest as sets of spatial-temporal partial differential equations (PDEs), posing numerical solvability challenges. Hence, linearized or reduced-order models and cable segmentation approximation techniques are commonly employed [6]–[8]. Additionally, spline collocation methods present another viable approach [14].

In [6], a mathematical multibody modeling approach for a cable slab is detailed, with the cable and hose assemblies represented as elastic beam elements. The equation of motion (EoM) is derived using nodal coordinates and deformation parameters, expressed as partial differential equations. Linearization of the EoM aids in determining the cable slab's bend geometry, albeit with significant computational demands. Experimental data and CAD files are utilized to estimate stiffness, with the resultant model showing promise for improving mechanical design and system control.

The work described in [7] delves into the application of absolute coordinates, enabling comprehensive capture of flexible hose non-linear kinematics. This approach facilitates the inclusion of bending-torsion and axial-radial couplings, enhancing the accuracy of the model. Particularly focusing on risers [7], the study explores the impact of internal fluid flow and friction arising from interactions with irregular seabeds.

This study primarily focuses on the motion of the cable slab within a plane. The key contributions are summarized as follows: Obtaining the kinematics and frequency response of the flexible cable slab at specific marker points, utilized as

[1]Department of Electrical Eng, Al-Zaytoonah University of Jordan, 130 Amman, 11733 Jordan, email:y.alrawashdeh@zuj.edu.jo
[2]Department of Mechanical and Mechatronics Eng, Memorial University, St. John's, NL A1B 3X5, Canada, email: {mialsaaideh, nalatawneh}@mun.ca
[3]School of Eng, University of Guelph, Guelph, ON N1G 2W1, Canada, email: {mpumphre,maljanai}@uoguelph.ca
[4]Department of Applied Mathematics, Czech Technical University, Prague, Czechia.

waypoints, to serve as training patterns for neural networks (NN). Capturing the dynamics of the flexible cable slab using two neural networks, namely coupled and decoupled networks. Approximating the bend geometry of the flexible cable slab using a cubic spline with time-varying coefficients, passing through the predicted positions of the waypoints obtained through the developed NN. Estimating the reaction force exerted by the moving end of the cable slab based on the developed NN, and proposing feedforward and feedback disturbance force compensation control strategies.

The paper is outlined as follows: the experimental setup and design details, providing insights into the practical implementation is documented in Section II. In Section III, the data-driven neural network model developed for the cable slab is outlined, presenting its structure and training process. Section IV addresses the estimation of cable slab-induced reaction forces and introduces our proposed feedforward disturbance compensation control scheme. Finally, concluding remarks and insights are presented in Section V, encapsulating the key findings and implications of this study.

II. Experimental Setup and Design

The experimental setup (depicted in Fig.1(a)) comprises equipment from PI (Physik Instrumente) L.P, including the A-322 PIglide HS XY Planar Scanner, operating with a resolution of $1, \mathrm{nm}$, an A-824 ACS Motion Controller with a cycle time of $0.5, \mathrm{ms}$ and a default frequency of $400, \mathrm{Hz}$, and three ironless zero-cogging brushless 3-phase linear motors in an H-configuration [1]. The gantry configuration is supported by a passive anti-vibration system from Thorlabs. The working space measures $500 \times 500, \mathrm{mm}^2$, with a maximum velocity and acceleration of $500, \mathrm{mm/s}$ and $5000, \mathrm{mm/s}^2$ respectively. The x-axis cable tray (depicted in Fig. 1(c)) is linked to the moving end of the y-axis cable slab, serving as the x-axis cable shuttle [6], [7]. This original cable slab facilitates air-bearing functionality and the transfer of electric power and feedback signals via flexible cables. To meet the objectives of this study, two additional experimental cable slabs, each with dimensions of $10\,\mathrm{mm} \times 60\,\mathrm{mm}$, are introduced along the x- and y-axis cable trays. Within these slabs, four unpressurized nylon hollow plastic tubes, a load cell (LC) cable, and a ribbon cable are incorporated (Fig. 1(c)). The load cell, interfaced via a suitable transducer (TR) to an NI USB-6008 data acquisition device from National Instruments (NI), has a capacity of $50, \mathrm{N}$ and a sensitivity of $1.906, \mathrm{mv/V}$. The H-configuration introduces coupling between the x and y axes when the x and y axes are in motion. This study focuses on modeling the x-axis experimental cable slab, with the y-axis kept stationary unless otherwise stated, utilizing the stay-pattern shown in Fig. 1(d).

In selecting cable slab configurations and materials, considerations such as technical environment, space restrictions, cycle frequency, required bending radius, and admissible motion kinetics are paramount. This study focuses on estimating cable slab disturbance forces and bend geometry under these requirements. To achieve this, variable sweeps

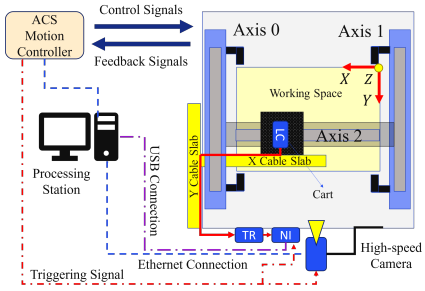

(a)

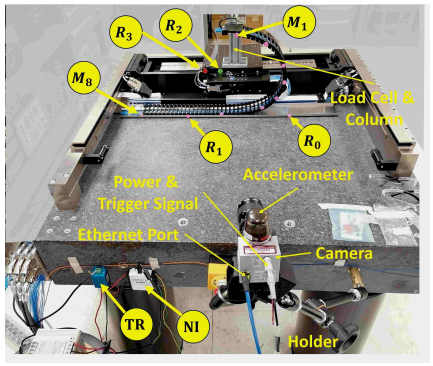

(b)

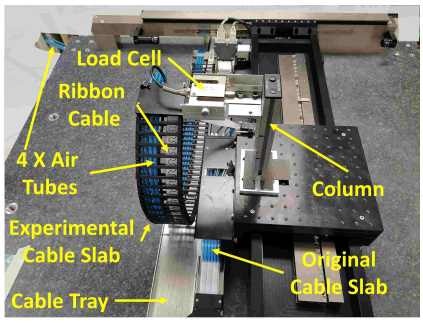

(c)

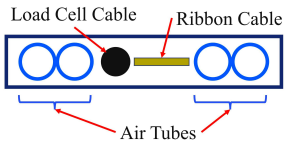

(d)

Fig. 1: Cable slab experimental (a) interaction diagram, (b) hardware, (c) the column assembly, and (d) the used experimental stay-pattern in the x-axis.

are conducted as detailed in Table I, utilizing cyclic motion profiles. Trapezoidal (PTP) and sinusoidal (BPTP) acceleration trajectories from the ACS controller enrich the experimental dataset. Tests 1 to 9 involve cyclic motion with strokes of $p_d \in [250, 500], \mathrm{mm}$, starting from the origin, with desired velocity $v_d \in [300, 500], \mathrm{mm/s}$, and acceleration $a_d \in [1000, 2000], \mathrm{mm/s}^2$, and a separation distance $d \in [180, 250, 310], \mathrm{mm}$ between fixed and moving ends of the cable slab. Throughout experiments, a common

TABLE I: The experimental setups for cyclic motion profiles.

Test #	Position $p_d\,(\mathrm{mm})$	Velocity $v_d\,(\mathrm{mm/s})$	Acceleration $a_d\,(\mathrm{mm/s^2})$	distance $d\,(\mathrm{mm})$
Test 1	500	500	2000	310
Test 2	500	300	2000	310
Test 3	250	500	1000	310
Test 4	500	500	2000	250
Test 5	500	300	2000	250
Test 6	250	500	1000	250
Test 7	500	500	2000	180
Test 8	500	300	2000	180
Test 9	250	500	1000	180

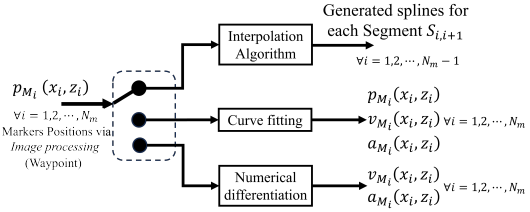

Fig. 2: The analysis of marker positions, acquired through the developed GNN image processing algorithm, conducted offline.

trigger signal synchronizes cart motion, camera recording, and load cell measurements, following a standard operating procedure (SOP) to minimize systematic errors and ensure consistency in experimental conditions.

In the experimental setup illustrated in Fig. 1(b), the ACS controller utilizes absolute encoders for cart position feedback, internally filtering velocity and acceleration data at a sample rate $f_s = 1000, \mathrm{sample/s}$. The cable slab reaction force is measured via an LC, converted by a TR to a voltage signal within $\pm 10, \mathrm{V}$, and interfaced to the processing station through an NI data acquisition device. Visual feedback is facilitated by a high-speed camera (HSC) from Fastec Imaging Corp, alongside the NI device and ACS motion controller, as depicted in Fig. 1(a). Additionally, a wireless triaxial G-Link-200 accelerometer from Parker Hannifin Corporation is affixed to the camera to monitor its pose and vibration relative to the motion stage. Synchronization across all devices is ensured via a common trigger signal issued by the ACS controller.

Alongside cyclic tests, we employ a random walk, or an acyclic, motion test. Here, we randomly select desired position $p_d \in [0, 500], \mathrm{mm}$, desired velocity $v_d \in [100, 500], \mathrm{mm/s}$, and desired acceleration $a_d \in [300, 5000], \mathrm{mm/s^2}$, with d manually fixed. This approach ensures comprehensive exploration of the cable slab's dynamic response.

Markers serve a crucial role in validating theoretical results obtained through numerical or analytical analysis [6], [8], with their locations aligning with the nodes used. Alternatively, if no prior analysis exists, markers can be strategically positioned to align with first or second flexible mode shapes in each segment. Remarkably, these markers can function as virtual sensors, offering kinematic measurements of the cable slab at designated locations, obviating the need for physical sensors like accelerometers [6]. This allows for both time and frequency domain analysis. In this study, $N_m = 8$ markers were arbitrarily placed along the cable slab.

The MATLAB Image Processing Toolbox is employed to detect markers in each captured frame after lens distortion correction. A red-green-blue (RGB) threshold color is utilized to isolate the bright circular markers during cyclic tests. Following marker position extraction using the GNN algorithm, additional data analysis is required to fulfill study objectives. Three post-processing steps, depicted in Fig. 2, are implemented for this purpose.

When dealing with mainly acyclic motion profiles, this process becomes essential. As acyclic motion lacks a predetermined pattern, numerical differentiation methods are employed to deduce marker kinematics from captured positions. In this study, the `diff` MATLAB function is utilized, with sampling rates determined by the FPS value. However, lower FPS values may result in noisy kinematics, while higher FPS values require increased disk storage space for offline data analysis. Hence, a trade-off must be considered in selecting the FPS value, with potential inclusion of suitable filters.

Under cyclic motion profiles, visual feedback allows for detection of patterns in marker positions $p_{M_i}(x_i(k), z_i(k))$, where $i \in 1, 2, 3, \ldots, 8$ and $k \in 1, 2, 3, \ldots, N$ denote frame and index numbers, respectively (with N being the total number of frames). With repeatable positions, velocity and acceleration profiles can be obtained through spatiotemporal interpolation across multiple frames [15]. To achieve this, the Fourier series model is employed to represent the position p_{M_i} of each marker along the x and z axes as

$$x_i(t) = a_{x0} + \sum_{j=1}^{q} a_{xj}\cos(jwt) + b_{xj}\sin(jwt), \quad (1)$$

$$z_i(t) = a_{z0} + \sum_{j=1}^{q} a_{zj}\cos(jwt) + b_{zj}\sin(jwt),, \quad (2)$$

where the coefficients a_{x0}, a_{xj}, b_{xj}, a_{z0}, a_{zj}, and b_{zj} are derived from markers position data in the k^{th} frame, where t represents the time of motion, and $q > 1$ is selected based on generated motion profiles. In this study, $q = 7$ is deemed suitable for the tests outlined in Table I. Consequently, velocity $(v_{M_i}(x_i(k), z_i(k)))$ and acceleration $(a_{M_i}(x_i(k), z_i(k)))$ for each marker M_i are computed by taking the first and second derivatives of the position down to any desired sampling rate, irrespective of the FPS value used.

Marker positions are represented in Cartesian coordinates, with each marker $M_i \ \forall i \in 1, 2, \cdots, N_m$ denoted by coordinates $(x_i(k),\ z_i(k))$ in the i^{th} frame. A cubic spline interpolation algorithm is then applied to spatially connect these markers, capturing the cable slab's bend geometry during operation. Specifically, the geometry of segment $S_{i,i+1}$ between markers M_i and M_{i+1} in the k^{th} frame is approximated using cubic splines as [14], [16].

$$\phi(x,k) = \sum_{j=0}^{3} \alpha_j^i(k)(x - x_{i+1}(k))^j,\ x \in [x_i(k), x_{i+1}(k)]\,, \tag{3}$$

$$\psi(z,k) = \sum_{j=0}^{3} \beta_j^i(k)(z - z_{i+1}(k))^j,\ z \in [z_i(k), z_{i+1}(k)]\,, \tag{4}$$

where spline coefficients $\alpha_j^i(k), \beta_j^i(k)$ for $j = 0, 1, 2, 3$ and $i = 1, 2, \cdots, N_m - 1$ in the k^{th} frame can be computed using MATLAB's `interp1` function. The bend geometry during cyclic and acyclic motion is then approximated using equations (3) and (4).

The cable slab response in segment $S_{i,i+1}, i = 1, 2, \cdots, N_m - 1$, can be mathematically approximated as a boundary value problem using the collocation method with piecewise polynomial functions when (3) and (4) are employed [14], [16]. Alternatively, other collocation methods utilizing trigonometric or power functions as linear combinations can also be utilized [17]. By strategically placing collocation points, i.e., markers, known behavior of the cable slab, such as first or second mode shapes, can be accurately reflected [16].

The bend geometry of segment $S_{i,i+1}, i = 1, 2, \cdots, N_m - 1$ in the k^{th} frame is determined by the $\alpha_j^i(k), \beta_j^i(k)$ coefficients, obtained using functions like `interp1`. At the coefficient level, the cable slab's spatiotemporal response is discerned. An example is depicted in Fig.3, showing the piecewise polynomial approximation of the cable slab response during Test 1 from an *uncorrected* image frame. However, in Fig. 3(b), the bend geometry between markers M7 and M8 dips below the x-axis cable tray (see Fig. 1(c)), which is physically implausible. This indicates insufficiency in the number of markers ($N_m = 8$) in this region, known for exhibiting seabed-like behavior [7] due to friction with the cable tray.

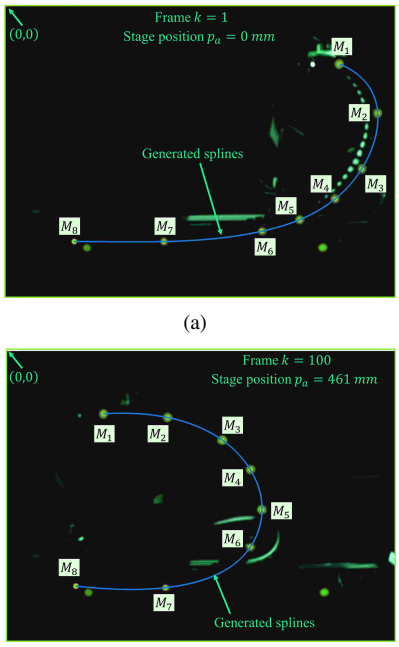

Fig. 3: The resulting piecewise cubic splines, created through interpolation during Test 1, are depicted in (a) at frame 1 (with the stage positioned at $p_a = 0$ mm) and in (b) at frame 100 (with the stage positioned at $p_a = 461$ mm).

III. Data-driven Model using Neural Network

This section introduces a data-driven model-based state-space (SS) neural network designed to capture the dynamic behavior of the cable slab using motion profile measurements provided by the ACS controller.

A. Modeling Formulation

The cable slab dynamic model can be formulated using state-space representation of the nonlinear system as

$$\dot{x} = f(x,u), \tag{5}$$

$$y = g(x,u) \tag{6}$$

where $x \in \mathbb{R}^n$ is the states of the system, $u \in \mathbb{R}^r$ is the input of the system, and $y \in \mathbb{R}^q$ is the output of the system.

In practice, deriving analytical equations to describe cable slab dynamics can pose challenges due to system complexity or limited domain knowledge. In such cases, data-driven modeling techniques like grey-box or black-box modeling offer valuable alternatives. Here, we employ a deep neural network state-space model (NN-SS) to represent both state and output equations of nonlinear systems, as depicted in Fig. 4.

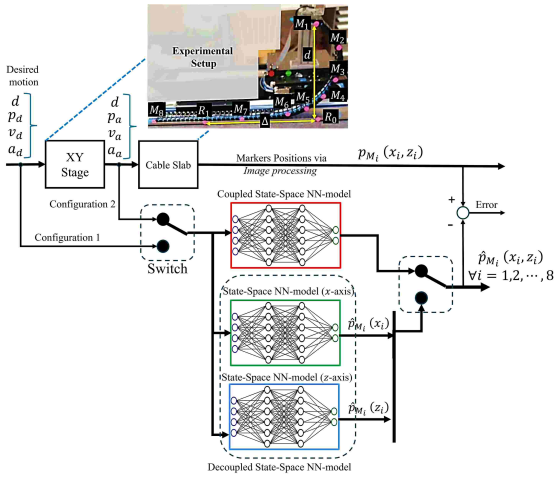

Fig. 4: Proposed state-space block diagram of the NN-based cable slab model (NN_1).

The NN-SS model employs a multi-layer perceptron (MLP) network to approximate both state and output equations. For the cable slab system under investigation, the output equation $y = x$ represents the marker's position along the x and z axes. Hence, a single NN-SS model suffices to describe the Cable Slab dynamics,

with network inputs being the state x and input u, and the network output being $\dot{x}$. MATLAB's Deep Neural Network and Identification toolboxes facilitate the design and training of the NN-SS model using built-in functions like `idNeuralStateSpace`, `createMLPNetwork`, and `nlssest`.

This study considers two configurations for the NN-SS, as depicted in Fig. 4. The first, the Coupled NN-SS model, comprises 4 inputs (actual position, velocity, acceleration of the stage (p_a, v_a, a_a), and distance d) and 14 outputs (position of each marker in both the x and z axes). The second configuration, the Decoupled NN-SS model, employs two separate NN-SS models: one for determining marker positions along the x-axis and another for the z-axis. Each model includes 4 inputs and 7 outputs. Both configurations feature two hidden layers with 100 and 50 neurons and use the `tanh` activation function.

The data collected from tests listed in Table I is employed to train the NN-SS model. Tests 1, 3, 4, 5, 8, and 9 contribute to the training dataset, while Tests 2, 6, and 7 are reserved for validation. Segmented into 100 samples for absolute error calculation, the training data utilizes the stochastic gradient descent with momentum solver, implemented via the MATLAB function `nssTrainingOptions('sgdm')`.

The proposed NN-SS model undergoes validation using Tests 2, 6, and 7 from Table I, which were unseen during training. Figures 5 and 6 depict the modeling error percentage between the marker positions obtained through image processing p_{M_i} and those estimated by the decoupled and coupled configurations of the NN-SS model $\hat{p}_{M_i}$. Notably, the model achieves an error of less than 3% in the x-axis and less than 5% in the z-axis marker positions relative to the maximum stroke motion. The obtained NN-SS is verified along the x-direction using acyclic motion as depicted in Fig. 7.

IV. Reaction Force Results

The cable slab reaction force can be estimated using the NN configurations depicted in Fig. 8. When employing d, p_d, v_d, a_d alongside load cell measurements F_c, the resulting neural network NN_2 finds application in the feedforward path, as discussed in works such as [9], [18]. Conversely, utilizing d, p_a, v_a, a_a and F_c leads to the utilization of NN_2 within an output feedback disturbance rejection control scheme following methods outlined in [19]. Upon removal of the load cell, the trained NN_2 serves to predict the exerted cable slab reaction force for any motion profile and d value. Similar to the approach taken with NN_1, the training and validation of NN_2 are conducted. It's important to note that at $d = 180, \text{mm}$, a reverse bending radius emerges, underscoring the necessity for adequate clearance above the cable slab to accommodate such cable bending.

The cable slab reaction forces exhibit variability dependent on the cart position, indicative of *position-dependent behavior*. Illustrated in Fig. 9 are such relationships under cyclic motion profiles outlined in Table I. For instance, Tests 1, 4, and 7 maintain the same operating point except for

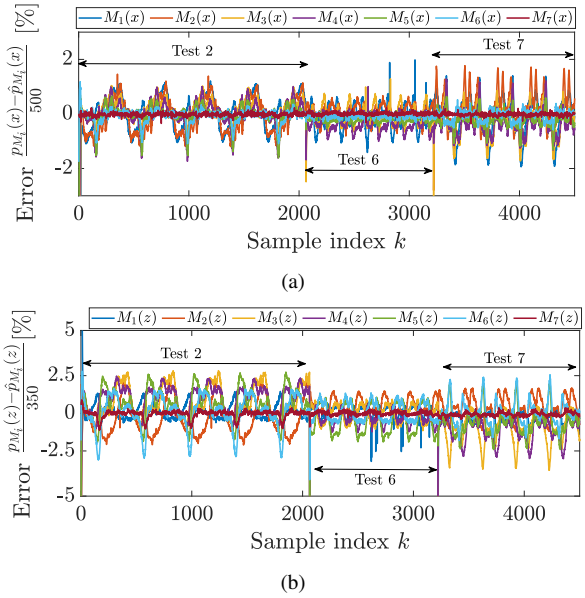

Fig. 5: The modeling error in marker motion is depicted for the decoupled configuration of the NN-SS model: (a) along the x-axis, and (b) along the z-axis.

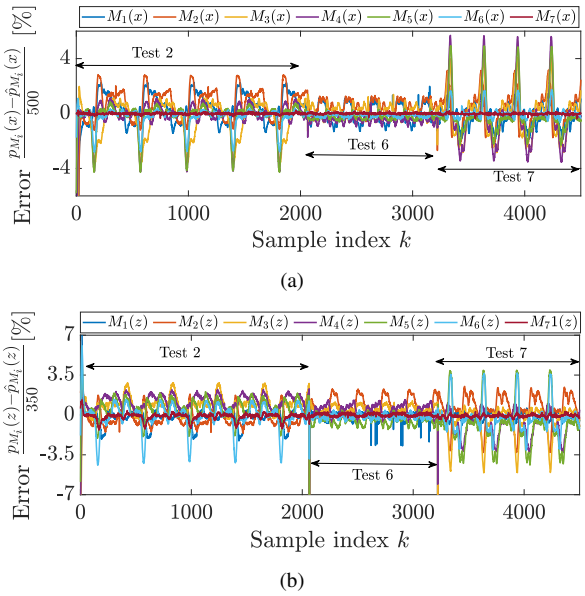

Fig. 6: The modeling error in marker motion is depicted for the coupled configuration of the NN-SS model: (a) along the x-axis, and (b) along the z-axis.

the d value, showcasing an increase in F_c as d decreases from $310, \text{mm}$ to $250, \text{mm}$ to $180, \text{mm}$. Similar trends are observed in Tests 2, 5, 8, and Tests 3, 6, 9. Altering only the velocity, as in Test 1 and Test 2, results in a decrease in F_c. Furthermore, reducing both acceleration and stroke length, as in Test 1 and Test 3, leads to a decrease in F_c, with diminished variation from forward to reverse paths. Examination of any point along the x-axis during testing elucidates the *path-dependent behavior* of the motion system,

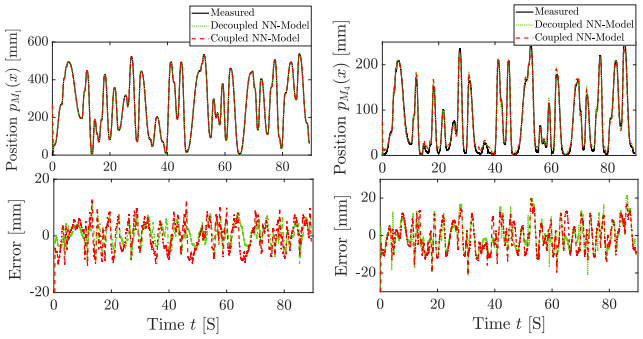

Fig. 7: Verification of the proposed state-space neural network (NN_1) for acyclic motion, conducted using the ACS controller built-in (BPTP) motion profile.

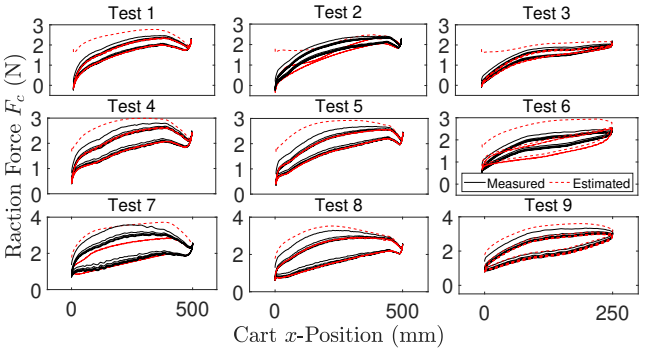

Fig. 9: The correlation between the cable slab reaction force F_c and the cart's x-position during the cyclic tests outlined in Table I is examined utilizing $p_a, v_a, a_a \rightarrow$ NN2 configuration.

attributable to F_c variation in either direction.

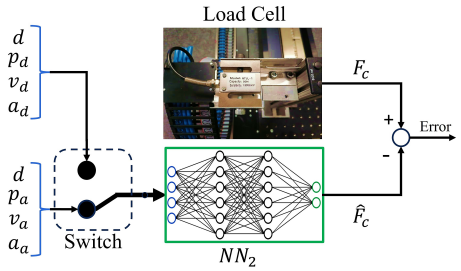

Fig. 8: Various configurations exist for training and employing NN_2 to estimate cable slab force, contingent upon signal availability and desired control scheme.

V. Conclusion

This study proposed a novel approach combining machine vision and neural networks to analyze cable slab dynamics, bend geometry, and reaction forces. By strategically positioning markers and utilizing a calibrated high-speed camera with advanced algorithms, marker positions in workspace coordinates are accurately tracked. These data serve as training patterns for neural networks, verified under both cyclic and acyclic motion profiles. Moreover, reaction forces exerted by the cable slab on the motion system are estimated using neural networks, enabling the proposal of two control configurations. This methodology offers a means to validate analytical results and digital twins against physical cable slabs in motion systems.

References

[1] Y. Al-Rawashdeh, M. Al Janaideh, and M. Heertjes, "On characterization of a generic lithography machine in a multi-directional space," *Mechanism and Machine Theory*, vol. 170, pp. 1–23, 2022.

[2] Y. Al-Rawashdeh, M. Heertjes, and M. Al Janaideh, "Motion orchestration in dual-stage wafer scanners," in *Proceedings of IEEE/RSJ International Conference on Intelligent Robots and Systems (IROS)*, pp. 8304–8309, 2023.

[3] Y. Al-Rawashdeh, M. Al Janaideh, and M. Heertjes, "On synchronization of generic lithography machine open-chains using a novel fine-positioning stage system," in *Proceedings IEEE Conference on Control Technology and Applications (CCTA)*, pp. 1089–1094, 2021.

[4] D. De Roover, F. Sperling, and O. Bosgra, "Point-to-point control of a mimo servomechanism," in *Proceedings of American Control Conference (ACC)*, pp. 2648–2651, 1998.

[5] J. Hyvärinen, M. Karlsson, and L. Zhou, "Study of concept for hydraulic hose dynamics investigations to enable understanding of the hose fluid–structure interaction behavior," *Advances in Mechanical Engineering*, vol. 12, no. 4, pp. 1–18, 2020.

[6] M. Hoogerkamp, R. Waiboer, and R. Aarts, "Modeling of flexible non-linear dynamic links in nano-positioning motion systems," in *Proceedings of Multibody Dynamics: ECCOMAS Thematic Conference*, pp. 287–296, 2013.

[7] Y. Chai and K. Varyani, "An absolute coordinate formulation for three-dimensional flexible pipe analysis," *Ocean Engineering*, vol. 33, no. 1, pp. 23–58, 2006.

[8] A. Sridhar, P. Tiso, and T. Hardeman, "A nonlinear model order reduction method for cable slab dynamics," in *Proceedings of International Conference on Noise and Vibration Engineering*, pp. 2611–2624, 2014.

[9] B. Xia, C. Yuan, Y. Tian, S. Wu, and K. Yang, "Disturbance estimation and compensation for planar motors on the long-stroke stage of a wafer stage," *Advances in Mechanical Engineering*, vol. 7, no. 4, 2015.

[10] J. Cho, Y. Yoon, C. Seo, and Y. Kim, "Fatigue life assessment of fabric braided composite rubber hose in complicated large deformation cyclic motion," *Finite Elements in Analysis and Design*, vol. 100, pp. 65–76, 2015.

[11] L. Merkle, M. Sonner, and M. Petzold, "Lifetime prediction of thick aluminium wire bonds for mechanical cyclic loads," *Microelectronics Reliability*, vol. 54, no. 2, pp. 417–424, 2014.

[12] J. Gbur and J. Lewandowski, "Fatigue and fracture of wires and cables for biomedical applications," *International Materials Reviews*, vol. 61, no. 4, pp. 231–314, 2016.

[13] R. Hoogeboom, "Design and experimental validation of low stiffness aerostatic thrust bearings," Master's thesis, Delft University of Technology, 2016.

[14] W. Schiesser, *Spline collocation methods for partial differential equations: With applications in R*. John Wiley & Sons, 2017.

[15] P. Revesz, *Spatiotemporal Interpolation Algorithms*, pp. 3646–3650. New York, NY: Springer New York, 2018.

[16] R. Russell and L. F. Shampine, "A collocation method for boundary value problems," *Numerische Mathematik*, vol. 19, pp. 1–28, 1972.

[17] J. Coleman and S. Duxbury, "Mixed collocation methods for $y = f(x, y)$," *Journal of computational and Applied Mathematics*, vol. 126, no. 1-2, pp. 47–75, 2000.

[18] R. G. Subramanian, M. Heertjes, and T. de Hoog, "A model-based inferential feedforward approach to deal with hysteresis in a motion system," in *Proceedings of American Control Conference (ACC)*, pp. 2934–2939, 2018.

[19] X. Shi and S. Chang, "Precision motion control of a novel electromagnetic linear actuator based on a modified active disturbance rejection controller," *Proceedings of the Institution of Mechanical Engineers, Part I: Journal of Systems and Control Engineering*, vol. 226, no. 5, pp. 606–614, 2012.